Altered excitability of cultured chromaffin cells following exposure to multi-walled carbon nanotubes.

Gavello D, Vandael DH, Cesa R, Premoselli F, Marcantoni A, Cesano F, Scarano D, Fubini B, Carbone E, Fenoglio I, Carabelli V.
Altered excitability of cultured chromaffin cells following exposure to multi-walled carbon nanotubes.
NANOTOXICOLOGY (2012) 6
DOI: 10.3109/17435390.2011.553294

Altered excitability of cultured chromaffin cells following exposure to multi-walled carbon nanotubes

DANIELA GAVELLO[1,2 §], DAVID H.F. VANDAEL[1 §], ROBERTA CESA[1,4], FEDERICA PREMOSELLI[1], ANDREA MARCANTONI[1,2], FEDERICO CESANO[2,5], DOMENICA SCARANO[2,5], BICE FUBINI[2,3,5], EMILIO CARBONE[1,2,4], IVANA FENOGLIO[2,3,5], VALENTINA CARABELLI[1,2,4]

1 Department of Neuroscience, University of Torino, 10125 Torino, Italy
2 Interdepartimental Center for Nanostructured Interfaces and Surfaces, Torino, Italy
3 Interdepartimental Center "G. Scansetti" for Studies on Asbestos and other Toxic Particulates, Torino, Italy
4 National Institute of Neuroscience, Torino, Italy
5 Department of Chemistry IFM, University of Torino, 10125, Torino, Italy

Corresponding authors:

Valentina Carabelli, Dept. of Neuroscience, Torino University, Corso Raffaello 30, 10125 Torino, Italy. Fax: +39 011 6708174. Email: valentina.carabelli@unito.it

Ivana Fenoglio, Dept. of Chemistry IFM, Torino University, Via P. Giuria 9, 10125 Torino, Italy. Fax: +39 011 6707577. Email: ivana.fenoglio@unito.it

§ These authors contributed equally to this work.

Abstract

We studied the effects of multi-walled carbon nanotubes (MWCNTs) on the electrophysiological properties of cultured mouse chromaffin cells, a model of spontaneously firing cells (Marcantoni al. 2010). The exposure of chromaffin cells to MWCNTs at increasing concentrations (30 to 263 μg/ml) for 24 h reduced, in a dose-dependent way, both the cell membrane input resistance and the number of spontaneously active cells (from 80% to 52%). Active cells that survived from the toxic effects of MWCNTs exhibited more positive resting potentials, higher firing frequencies and unaltered voltage-gated Ca^{2+}, Na^{+} and K^{+} current amplitudes. MWCNTs slowed down the inactivation kinetics of Ca^{2+}-dependent BK channels. These electrophysiological effects were accompanied by MWCNTs internalization, as confirmed by transmission electron microscopy, indicating that most of the toxic effects derive from a dose-dependent MWCNTs-cell interaction that damages the spontaneous cell activity.

Keywords: MWCNTs, voltage-gated Na^{+} and K^{+} channels, Ca^{2+} and BK channels, adrenal chromaffin cells, action potential firing, input resistance.

Introduction

The interest in nanomaterials is rapidly increasing because of their potential application in biomedicine, cosmetics, electronics, sport goods, mechanics and other manufactured items (Nel et al. 2006), thus leading to a parallel rising of the social concern on their effects on human health. Carbon nanotubes (CNTs) are among the most widely studied nanomaterials because of their unique physical, chemical and mechanical properties, but they are also considered one of the most potentially harmful nanomaterials to humans (Kane and Hurt 2008; Lam et al. 2006). Carbon nanotubes (CNTs) are cylindrical structures formed by one (single-walled SWCNTs) or more (multi-walled MWCNTs) bent graphene layers of variable length, even above 5 μm, but with diameter in the nanometer range. Depending upon the methods of production and purification, CNTs may largely differ in form, impurities (metals, amorphous carbon) and defects. CNTs have been the matter of debate as several *in vivo* and *in vitro* studies have shown that CNTs may trigger toxic effects, as reported in recent reviews (Donaldson et al. 2009; Lam et al. 2006; Lison et al. 2008; Shvedova et al. 2009). In some cases they have been reported to cause asbestos-like damage (Poland et al. 2008; Takagi et al. 2008).

The nature of their toxicity is still highly debated (Kane and Hurt 2008) and mostly focused on their potential lung toxicity, particularly on airways and mesothelium. Only few data are available on other organs and cell types, including toxic effects of CNTs on nervous tissues. Several types of nanoparticles have been reported to reach the central nervous system through sensory and olfactory nerve pathways (Elder et al. 2006; Oberdörster et al. 2001; Oberdörster et al. 2004), or translocate from the lung to the blood stream (Kreyling et al. 2002; Nemmar et al. 2001; Oberdörster et al. 2002). There is no clear evidence that CNTs may migrate in extra-pulmonary organs following intratracheal instillation (Al Faraj et al. 2009; Deng et al. 2007; Elgrabli et al. 2008). However, recently, Ryman-Rasmussen and

collaborators reported that CNTs may reach the subpleural tissue in mice, moving rapidly through the alveoli epithelium (Donaldson et al. 2009; Ryman-Rasmussen et al. 2009). So far, *in vitro* effects of single-walled (SWCNTs) and multi-walled carbon nanotubes (MWCNTs) on neurons have not been throughly investigated. The few available data concern the toxic effects of SWCNTs on dorsal root ganglion (DRG) neurons (Belyanskaya et al. 2009), the blocking of neuronal Ca^{2+} channels by micromolar concentrations of yttrium released from SWCNTs (Jakubek et al. 2009), the direct blocking of various K^+ channels by SWCNTs in chinese hamster ovary (CHO) cells (Park et al. 2003) and the suppression of K^+ channel activity in PC12 cells, induced by carboxy-terminated MWCNTs (Xu et al. 2009).

Here we studied the dose-dependent effects of well characterized multi-walled carbon nanotubes on neuroendocrine cells. Our study focuses on the basic electrophysiological properties of adrenal chromaffin cells after MWCNTs exposure, representing a suitable model of neuronal-like excitable cells, with particular interest to their neuroendocrine function. We addressed this by means of electrophysiological trials and electron microscopy assays, to monitor MWCNTs-cell interaction, MWCNTs internalization and MWCNTs-induced alterations of ionic conductance mechanisms controlling chromaffin cell excitability. We found that increasing doses of MWCNTs reduce the number of spontaneously firing cells in a dose-dependent manner without altering the voltage-gated Na^+, Ca^{2+} and K^+ channels. This is likely due to the MWCNTs-cell interactions occurring during the 24 h time exposure that lower the cell resistance and resting membrane potential and induce marked alterations to cell excitability.

Materials and Methods

Preparation and physico-chemical characterization of CNTs

Multi-walled CNTs were purchased by Mitsui Chemicals (Kawasaki-Shi, Japan). To improve

the dispersibility in the culture media CNTs were ground in an oscillatory ball mill during 6 hours.

The dimension of CNTs has been evaluated directly by means of transmission electron and scanning electron microscopies. The statistical evaluation of diameters and lengths of the MWCNT fragments was obtained by considering a population of 213 data points for each sample, from low resolution TEM images of the ground sample (4000X and 25000X as magnification, respectively). TEM images were collected by a JEOL 3010-UHR TEM instrument operating at 300 kV.

The surface area of CNTs has been measured by means of the B.E.T (Brunauer, Emmett and Teller) method based on N2 adsorption at -196ºC (ASAP 2020 Micrometrics, Norcross, GA 30093-2901, U.S.A.). For the elemental analysis, the samples were heated at 700°C in a furnace and the residue dissolved in 37% HCl. The concentration of iron in the solution was quantified by atomic emission-ICP spectrometry (IRIS II Advantage/1000, Thermo Jarrel Ash).

Evaluation of potentially bio-available iron

This test was performed to evaluate the amount of iron ions which may be exposed at the surface of the MWCNTs. For this purpose, a strong chelator (ferrozine®) and a reducing agent (ascorbic acid) were used to extract iron ions. 25 mg of the powders were incubated in 10 ml of a 3 mM solution of ascorbic acid and ferrozine. After 10 days an aliquot of the supernatant was withdrawn after centrifugation and the concentration of iron evaluated my measuring the absorbance at 562 nm (typical of the complex ferrozine-Fe(II)) with a UV/Vis spectrophotometer (Uvikon, Kontron, spectrophotometer). The amount of extractable iron is reported on Table 1.

Raman spectroscopy

Micro-Raman spectra were acquired using an integrated micro/macro Raman system which includes a Horiba Jobin Yvon HR800 microspectrometer, an Olympus BX41 microscope and a CCD air-cooled detector. A polarized solid state Nd 80 mW laser operating at 532.11 nm was used as the excitation source. Calibration of the instruments was performed by measuring the Stokes and anti-Stokes bands and checking the position of the Si band at ± 520.7 cm-1. Each spectrum was acquired using a 100X objective, resulting in a laser beam size at the sample in the order of 2 mm. To optimize the signal to noise ratio, spectra were acquired using 10 scans of 10 seconds for each spectral region. In order to produce strong signals without inducing surface alteration due to the heat, a filter with optical density d = 0.6 was used. The software LabSpec 5 (Horiba Jobin Yvon) was used to analyze the spectra. The ID/IG value is the ratios of the intensities of two bands designated as D (1340 cm-1) and G (1570 cm-1) which correspond respectively to structural defects and to the tangential in-plane stretching vibration of the carbon-carbon bonds within the graphene sheets.

Dispersion of MWCNTs in the culture media

MWCNTs were suspended in the culture media at three different concentrations: 263 μg/ml, 100 μg/ml and 30 μg/ml. The suspensions were sonicated two times for 2 minute with a probe sonicator (100 W, 20 kHz, Sonoplus, Bandelin, Berlin, Germany). Average hydrodynamic size of MWCNTs in the culture media has been evaluated by means of dynamic light scattering (DLS), (Zetasizer Nano–ZS, Malvern Instruments, Worcestershire, U.K.) for the sample at higher concentration (263 μg/ml) . The measurement was repeated after 15 minutes to evaluate the stability of the suspension. Since in the DLS technique aggregates larger than 10 μm are not detected, optical microscopy was also used to detect the presence of large aggregates.

As a negative toxicity control we used a sample of tris(dicarboxymethylene)fullerene (Vinci-Biochem) dissolved in the culture medium at the concentration of 263 µg/ml.

To evaluate the effects of MWCNTs on the concentration of proteins in the cellular media, MWCNTs were suspended in a 15% fetal bovine serum aqueous solution for 48 hours and then removed by centrifugation. The total amount of proteins which remained in the supernatant was measured spectrophotometrically by means of bicinchoninic acid (BCA) assay and compared with the control solution (Smith et al. 1985).

Isolation and culture of chromaffin cells

Mouse chromaffin cells (for electrophysiology): mouse chromaffin cells were obtained from young C57BL/6J male mice, which were killed by cervical dislocation and cultured following the method of Sørensen (Sørensen et al. 2003), with minimal modifications. After removal, the adrenal glands were placed in Ca^{2+}- and Mg^{2+}-free Locke's buffer containing (in millimolar): 154 NaCl, 3.6 KCl, 5.6 $NaHCO_3$, 5.6 glucose, and 10 HEPES, pH 7.3, at room temperature. The glands were decapsulated, and the medullas were precisely separated from the cortical tissue. Medulla digestion was achieved after 50 min at 37°C in the enzyme solution (0.16 mM L-cysteine, 1 mM $CaCl_2$, 0.5 mM EDTA, DMEM) containing 20 U/ml of papain (Worthington Biochemical, Lakewood, NJ, USA) plus 0.1 mg/ml of DNAse (Sigma). The cell suspension was then washed twice with a washing solution (DMEM, 1 mM $CaCl_2$, 10 mg/ml BSA), and resuspended in 2 ml DMEM supplemented with 15% fetal bovine serum (FBS). Cells were plated in four-well plastic dishes treated with poly-L-ornithine (0.5 mg/ml) and laminin (10 µg/ml in L-15 carbonate) by placing a drop of concentrated cell suspension in the center of one well. After 1 h, 1.8 ml of DMEM supplemented with 15% FBS (Invitrogen, Grand Island, NY, USA), 50 IU/ml penicillin, and 50 µg/ml streptomycin (Lonza), 10 µM Cytosine b-D-arabino-furanoside-hydrochloride (Sigma), 10 µM 5-Fluoro-

2'-deoxyuridine (Sigma) was added to the wells. Cells were then incubated at 37°C in a water-saturated atmosphere with 5% CO2 and used within 2–6 days after plating. All experiments were performed in accordance with the guidelines established by the National Council on Animal Care and were approved by the local Animal Care Committee of Turin University.

Rat chromaffin cells (for electron microscopy): the preparation was obtained as explained before for mouse chromaffin cell culture, with the exception of papain, which was substituted with a solution of liberase-blendizymes-3 at the concentration of 0.35 mg/ml (Roche). Thus, 100 µl of lyberase solution were added for each ml of DMEM.

Electrophysiology

Voltage-clamp and current-clamp experiments: Ca^{2+} currents were recorded in perforated-patch recording conditions using an EPC-9 patch-clamp amplifier (HEKA Elektronik, Lambrecht, Germany). Patch pipettes were made of thin borosilicate glass (Kimax 51; Witz Scientific, Holland, OH, USA) and filled with an internal solution containing (in millimolar): 135 $CsMeSO_3$, 8 NaCl, 2 $MgCl_2$, 20 HEPES, pH 7.3, with CsOH plus amphotericin B (Sigma). The external bath contained (in millimolar): 128 NaCl, 10 $CaCl_2$, 2 $MgCl_2$, 10 glucose, 10 HEPES, 4 KCl, 2 TEACl, pH 7.4, with NaOH. Amphotericin B was dissolved in dimethyl sulfoxide stored at −20°C in stock aliquots of 50 mg/ml and used at a final concentration of 500 µg/ml. To facilitate the sealing, the pipette was first dipped in a beaker containing the internal solution and then back-filled with the same solution containing amphotericin B. Pipettes with series resistance of 1–2 MΩ were used to form giga-seals. Series resistance was compensated by 80% and monitored throughout the experiment. K^+ currents were also recorded in perforated-patch conditions, using an internal solution containing (mM): 135 KAsp, 8 NaCl, 20 Hepes, 2 $MgCl_2$ and 5 EGTA. As external solution

we used a normal physiological Tyrode's solution with the following composition (in mM): 130 NaCl, 4KCl, $2CaCl_2$, $2MgCl_2$, 10 HEPES and 10 glucose adding 300 nM TTX in order to block the sodium current. Also the current-clamp experiments were performed by means of the perforated patch method. The intracellular solution contained in mM: 135 KAsp, 8 NaCl, 20 Hepes, 2 $MgCl_2$ and 5 EGTA. As an extracellular solution for the current clamp experiments we used a normal physiological Tyrode's solution.

Regarding the input resistance meaurements we used the same solutions described above for current clamp experiments.

Electron microscopy

Chromaffin cells were cultured on Aclar Fluoropolymer film (Electron Microscopy Sciences, USA) following the protocol explained before. After 24/48 h of treatment, cells were fixed for 1 hour with 2% glutaraldehyde in PBS at room temperature, washed with cacodylate buffer, post-fixed in 1% osmium tetroxide in cacodylate buffer for 1 hour in ice and dehydrated in gradient ethanol, followed by propylene oxide. Samples were then embedded in Epon-Araldite. Ultrathin sections (80-100 nm) were cut with a diamond knife on an ultramicrotome (Leica Microsystems, Germany) and collected on Pioloform-coated single slot grids (Electron Microscopy Sciences, USA). Sections were stained with uranyl acetate and lead citrate and examined in a JEM-1010 electron microscope (Jeol, Japan) equipped with a side-mounted CCD camera (Mega View III; Soft Imaging System, Germany). To determine whether the nanotubes could be present inside the cells, approximately 50 chromaffin cells treated with MWCNTs for 24 and 48 h were randomly examined. The percentages of internalization were calculated considering the number of cells that internalized MWCNTs as 100% for each group (24 h and 48 h).

Results

Physico-chemical properties of MWCNTs

One of the major flaws of the available data on MWCNTs toxicity is the poor physico-chemical characterization of the samples, which makes difficult any comparison, among different studies. Moreover the lack of correlation between physico-chemical properties and induced toxic effects deprives material chemists of the possible clues for the design of safer products (Fubini et al., 2010). In this study, a sample of commercial MWCNTs (Mitsui Chemicals, Kawasaki-Shi, Japan) having 0.27 % iron impurities has been ground in a ball mill in order to shorten the length of tubes and improve the dispersibility in physiological media. It is noteworthy that by moving from the commercial material to the ground one a p rupture in the carbon nanotubes structure takes place with consequent increase in the specific surface area, likely following the opening of the internal pores and the formation of irregular terminations (Table 1).

Ground MWCNTs consist of bundles of short straight tubes having a mean diameter of 67 ± 2 nm and a mean length of 1.12 ± 0.5 μm (Fig. 1, Table 1). From this image a few rounded agglomerates of carbon particles, together with more dark regions at the borders of the nanotubes are observed. These thickness differences can be explained with interlayer spacing defects, i.e. stacking faults, plausibly arising from the ground process. The opening of some isolated fragments is also imaged, as evidenced from the enlarged view shown in the inset of figure 1. The grinding process also introduces reactive defects following the cleavage of C-C bonds. Raman spectroscopy provides a useful method to broadly evaluate the extent of defects present in CNT (Jorio et al. 2004; Osswald et al. 2007; Fenoglio et al. 2008). In the Raman spectra of the pristine and ground MWCNTs (Fig. 2) two main bands are visible: the band designated as D (1340 cm^{-1}) is associated to structural defects while the bands G (1570 cm^{-1}) is due to the tangential in-plane stretching vibration of the carbon-carbon bonds

within the graphene sheets. The ratios of the relative intensities of the D and G bands (I_D/I_G) may be confidently used to estimate variations in the concentration of defects. The pristine samples exhibited a very low I_D/I_G value (Table 1) which corresponds to a high degree of crystallinity. As expected, the I_D/I_G value increased upon grinding, confirming the formation of defects under mechanical stress. In a previous study such defects have been shown to affect the inflammogenic and genotoxic potential of MWCNTs (Fenoglio et al. 2008; Muller et al. 2008) but not their cancerogenicity (Muller et al. 2009). The sample contains trace levels of iron as impurity which is almost totally exposed to the solvent, thus bioavailable (Table 1) (Guo et al. 2007; Liu et al. 2008). The presence of rare iron particles, whose diameters range in the 0.2 ÷ 2 μm interval, is also confirmed from TEM and SEM images, not reported here for sake of brevity.

Being highly hydrophobic, CNTs are not well dispersed in aqueous media, therefore different protocols for the preparation of stable suspension have been proposed (Elgrabli et al. 2007; Yu et al. 2007). Here, we dispersed CNTs directly in the cellular media (263 μg/ml) supplemented with 15% fetal bovine serum (FBS) as detailed explained in Materials and Methods. The presence of proteins is known to improve the dispersion of MWCNTs (Elgrabli et al. 2007) most probably acting as surfactants. The degree of dispersion and the stability of the suspensions were evaluated by means of dynamic light scattering technique (DLS) (Fig. 3a). The single peak corresponds to particles having an equivalent hydrodynamic diameter of 300 nm that could be due to both, single CNTs or small agglomerates. Since this technique has an upper limit resolution of 1 μm, the presence of larger aggregates was confirmed by optical microscopy (Fig. 3b). CNTs appear uniformly distributed in the suspension with some aggregates having diameters of 1-5 μm. The stability of the suspension was followed for 15 min, which is sufficient for a correct dosage.

Note that the addition of MWCNTs did not significantly modify the concentration of

total proteins in the media (see Materials and Methods).

MWCNTs are internalized in chromaffin cells

A first set of electron microscopy trials has been performed with the aim of assessing whether nanotubes could be internalized in chromaffin cells, as shown in human epidermal keratinocytes (Monteiro-Riviere et al. 2005) and other works focused on the cellular uptake of CNTs (Raffa et al. 2010). In order to simplify the experimental procedure, for these experiments we used rat chromaffin cells (RCCs) instead of mouse (Fig. 4a-d). RCCs were exposed to 263 μg/ml MWCNTs dispersed in the culture medium as previously described, for 24 and 48 h and then cut in ultrathin sections of 80-100 nm thickness. In both groups of cells (24 and 48 h treatment) MWCNTs crossed the plasma membrane and were clearly visible inside the cells (Fig. 4b-d). The nanomaterial was present in 78% of cells after 24 h and 80% after 48 h exposure at 263 μg/ml concentration (Fig. 4e). In particular, single nanotubes (white square in panel b and arrows in panels d) and aggregates (dashed white lines in panels b and c) were already visible inside the cells after 24 h, while after 48 h there was a predominance of aggregates. Among those cells exhibiting internalization after 48 h exposure to MWCNTs, 78% contained nanotubes as agglomerates and just 22% contained single nanotubes (Fig. 4f), suggesting that percentage of aggregation increased with time. These findings demonstrate that MWCNTs are able to cross the plasma membrane and reach both the cytoplasm (Fig. 4c and d) and the nuclear membrane (Fig. 4). Especially after prolonged exposure (48 h) they can disrupt the internal organization of the cell (Fig. 4c). In this case, organelles are no longer visible and the cytoplasm appears rich of MWCNTs aggregates (dashed white square). These results are in agreement with previous reports (Kostarelos et al. 2007), suggesting that CNTs probably penetrate the cells due to their long and thin shape, crossing the plasma membrane as a “nanosyringe”. Interestingly, we found that the

internalization process is not limited to the plasma membrane but proceeds up to the nucleus (N) (Fig. 4b), with possible adverse effects at the genomic level.

MWCNTs reduce the number of spontaneously active chromaffin cells

Isolated chromaffin cells from the adrenal gland are spontaneously firing (Marcantoni et al. 2010). The goal of our study was to understand whether the exposure to MWCNTs for 24 hours could interfere with the generation of action potentials (Marcantoni et al. 2009). By means of current-clamp perforated-patch recordings, we compared the spontaneous activity of MCCs in control conditions and after exposure to increasing concentrations of MWCNTs (from 30 μg/ml to 263 μg/ml). Control MCCs exhibited spontaneous firing activity in 80% of cases (n=33). On the contrary, exposure to MWCNTs for 24 h reduced the number of spontaneously firing MCCs in a dose-dependent manner. The lower dose of MWCNTs (30 μg/ml) reduced the number of firing cells to 67% (n=21) while higher concentrations (100 μg/ml and 263 μg/ml), reduced the number of firing cells to 48% (n=25) and 52% (n=29), respectively (Fig. 5a). This clearly indicates that MWCNTs affect MCCs functioning. To clarify if the observed effect was specific for MWCNTs, cells were exposed to 263 μg/ml of a carboxymethylene derivative of fullerene, which shares with CNTs the same chemical nature but not their fibrous shape. This material has been previously reported to be non-toxic toward neuronal cells (Dugan et al. 1997; Lin et al. 1999). In this case the percentage of active chromaffin cells (80%, n=14) was not significantly different from controls.

MWCNTs reduce the membrane input resistance of chromaffin cells

Since the loss of function of chromaffin cell activity could be due to a MWCNTs-cell interaction damaging the cell membrane integrity, we next monitored the membrane input resistance. We quantified this parameter by applying a small hyperpolarizing current pulse (-

10 pA) of 100 ms duration from resting potential and then measuring the induced voltage change (ΔV; Fig. 5b). On average, the cell input resistance of MCCs after exposure to MWCNTs was smaller if compared to controls (grey vs. black trace in Fig. 5b): mean input resistance was 2.1 ± 0.3 GΩ (either with 100 or 263 μg/ml MWCNTs) versus 3.3 ± 0.1 GΩ in control ($p < 0.01$). On the contrary, neither the treatment for 24 h with fullerenes (2.9 ± 0.4 GΩ; n=4) nor with MWCNTs 30 μg/ml (2.9 ± 0.2 GΩ; n=7), induced a significant reduction of membrane resistance as compared to controls ($p > 0.05$). The cell input resistance decreased in a dose-dependent manner with an IC_{50} of 37.0 ± 0.5 μg/ml and a Hill slope of 3.5 ± 0.2 (fig. 5c).

We also found that the percentage of firing cells was linearly correlated with the cell input resistance values (Fig. 5d, R= 0.99), suggesting that exposure to increasing MWCNTs concentrations reduces the membrane integrity (increases background leakage currents) and affects cell excitability.

When spontaneous firing is not abolished by MWCNTs, the firing frequency increases

Next we monitored the firing frequency of those cells whose spontaneous firing activity was not suppressed by MWCNTs treatment. Figure 6a shows the spontaneous activity of representative control cell, after treatment with fullerenes (263 μg/ml) and with MWCNTs at the maximal concentration (263 μg/ml).

In the three groups of MWCNTs-treated cells (using 30, 100 and 263 μg/ml), the spiking frequency showed a tendency to increase with increasing MWCNTs concentration. The highest discharge rate (1.00 ± 0.18 Hz) was observed when applying the maximal MWCNTs concentration (263 μg/ml, n= 7, $p < 0.05$) while at lower concentrations there was no significant difference compared to controls. Firing frequency decreased to 0.8 ± 0.2 Hz (n= 7) or 0.60 ± 0.18 Hz (n= 9) for 100 μg/ml and 30 μg/ml MWCNT, respectively. Controls and

cells treated with fullerenes fired at 0.63 ± 0.07 Hz (n= 26) and 0.69 ± 0.12 Hz (n= 8), respectively (Fig. 6a). Increasing doses of MWCNTs caused also a reduction of the action potential (AP) amplitude that reached minimal values at 100 µg/ml MWCNTs (70 ± 2.2 mV; n=6, p<0.05), whereas was indistinguishable from control values (76.9 ± 1.2 mV; n= 25) with fullerenes (Fig. 6b).

We next examined how the interspike (resting) potential changed after exposure to different MWCNTs concentrations. The results revealed more depolarized values in the presence of carbon nanotubes in the medium. In control MCCs and with fullerenes, interspike potential values were statistically indistinguishable (–47.2 ± 0.7 mV; n= 26 and –46.9 ± 0.8 mV; n= 9). On the contrary, MCCs incubation with MWCNTs induced a shift of the resting potential to more positive values, proportional to the rise of MWCNTs concentration. Cells treated with 30 µg/ml had membrane resting potentials comparable to controls (–47.4 ± 1.5 mV; n= 9), while MCCs exposed to 100 µg/ml had significantly lower values: –42.5 ± 0.6 mV (n= 7; p< 0.05). This trend persisted with 263 µg/ml CNTs. Fig. 6c shows the linear relationship existing between firing frequency (Hz) and membrane resting potential (interspike value) (mV), in control and at different MWCNTs concentrations (R= 0.74), while fig. 6d shows that firing frequency increases with increasing MWCNT concentrations, to reach nearly twice the control value at 263 µg/ml MWCNTs (0.63 ± 0.07 vs. 1.00 ± 0.18 Hz; p< 0.05). In conclusion, MWCNTs act on MCCs by lowering the resting membrane potential, the action potential amplitude and increasing the rate of firing.

MWCNTs do not alter Na^+, Ca^{2+} and voltage-gated K^+ currents and slow-down BK currents inactivation

The changes of firing frequency, AP amplitude and resting potential could be due to a selective action of MWCNTs on one or more of the ion channel conductances controlling the

resting potential and spontaneous activity of MCCs. For this reason, we first tested whether the effects of 24 h exposure to MWCNTs were on voltage-gated Na^+ and Ca^{2+} currents by using the *voltage-clamp* technique (Fig. 7a). Steady-state Ca^{2+} current amplitudes (Fig. 7b) and quantity of Ca^{2+} charges entering the cell during 100 ms depolarizing pulses (Fig. 7c) were measured from –50 to +40 mV and appeared unaffected by MWCNTs-treatment. A lack of effects was also observed on the peak Na^+ currents, which was of –0.9 ± 0.2 nA in control conditions and –1.2 ± 0.2 nA at 0 mV with MWCNTs (Fig. 7d). In good agreement with the observation that during spontaneous firing the AP overshoot was preserved after MWCNTs exposure. Taken together these findings suggest that MWCNTs had no evident effects on the size of Na^+ and Ca^{2+} currents which are responsible for pacemaking the firing and shaping the fast AP depolarization in MCCs (Marcantoni et al. 2009; Marcantoni et al. 2010).

Next we measured the effects of MWCNTs on K^+ channel conductances. MCCs express at least two types of K^+ channels which contribute to shape and affect the AP frequency: the voltage-gated (K_v) and the Ca^{2+}-activated Big-K^+ (BK) channels (Marcantoni et al. 2010). Ion currents flowing through these open channels are mostly evident using an external solution containing TTX (300 nM) to block inward Na^+ currents and double-pulse stimulation protocols, consisting of a long step depolarization to +80 mV followed, after 10 s interval, by a second pulse to +80 mV, preceded by a short pre-step of 20 ms to 0 mV. The first pulse allows estimating the size and time course of voltage-gated K^+ currents, while the second pulse induces sufficient intracellular Ca^{2+} loading to activate a large fraction of the Ca^{2+}-dependent BK currents (Fig. 8a). Separation of K_v and BK currents was confirmed using paxilline (a selective BK channel blocker; Marcantoni et al. 2010), which abolishes the exceeding K^+ current activated during the short pre-step (recordings in panel b and c, bottom).

We found that in control MCCs, BK channels undergo rapid and rather complete inactivation

(black trace in Fig. 8b-top) while in cell pre-treatment with MWCNTs, inactivation was slower and largely incomplete (black trace in panel c-top). The peak value of BK currents (BK_p) remained nearly unchanged (3.5 ± 0.4 nA in control vs 3.0 ± 0.3 nA with MWCNTs; black boxes in panel b and c) while the steady-state value of the BK current measured at the end of the pulse (BK_{ss}) increased by nearly a factor 8: from 0.3 ± 0.1 nA to 2.2 ± 0.4 nA (white boxes in panel b and c). As shown to the left, the size of K_v currents was unaffected by MWCNTs-treatment, indicating that the main effect of MWCNTs was a slowing down of BK channel inactivation. This effect could be ascribed to an increased intracellular Ca^{2+} charge associated to the damaged cell membrane after MWCNTs exposure (decreased membrane resistance and increased background leakage current). In conclusion, the voltage-clamp data suggests that MWCNTs do not significantly alter the main ionic conductances that are responsible for AP generation and spontaneous firing of MCCs (Marcantoni et al. 2010; Vandael et al. 2010): the voltage gated Na^+ , Ca^{2+} and K^+ and the BK channels, except for a prolongation of BK channel inactivation. This implies that most of the toxic effects of MWCNTs after 24 h exposure to concentrations above 30 µg/ml derive from the decreased cell membrane resistance (increased leakage) and more depolarized resting potentials, which drives the MCCs either to stop their activity or remain active at higher firing frequencies.

Discussion

The main novelty of the present findings is that the toxic effects of long-term exposure to different doses of MWCNTs on excitable cells may not simply derive from a depressive action on Na^+, K^+ and Ca^{2+} currents, as previously reported (Jakubek et al. 2009; Park et al. 2003; Xu et al. 2009; Belyanskaya et al., 2009), but could be the consequence of a damage involving the cell membrane. After 24 h incubation, MWCNTs enter chromaffin cells as shown by the electron microscopy images and indicated by the reduced input resistance of the

plasmamembrane, without any preferential cytoplasmic localization. This effect led us to suppose that most likely MWCNTs are taken up by chromaffin cells by creating small pores into the lipid bilayer, allowing the passage of unspecific ion currents. However, it is worth to be mentioned that the process of nanoparticles internalization may occur through different pathways, depending on cell type, size and bundling of carbon nanotubes. Functionalized carbon nanotubes can cross the membrane through phagocytosis, or may penetrate the plasma membrane and be transported towards the perinuclear region, even under endocytosis-inhibiting conditions (Kostaleros et al. 2007). Also, nanoparticles can form receptor-bound complexes and be endocytosed (Jin et al. 2009), as demonstrated by tracking their intrinsic photoluminescence.

The presence of cellular damage, after MWCNTs exposure, is also suggested by the reduced number of MCCs with spontaneous firing activity. The reduction of the input resistance values after MWCNTs incubation could be due to the presence of more unspecific open channels (background leakage), compared to controls, or to the presence of pores induced by the entrance of the nanomaterial. In order to solve this question we measured the amplitude of voltage-gated Na^+ Ca^{2+} and K_v^+ channels, and we found that MWCNTs exposure did not induce any change in the conductance of any of these channels. The only conductance that was substantially changed was the paxilline sensitive Ca^{2+} activated BK current, which is more slowly inactivating. Since no changes in the total Ca^{2+} channel conductance have been observed in MWCNTs treated cells, we hypothesized that this BK current might be affected by calcium entering the cell through non-selective ionic pathways (MWCNTs induced pores). Overall, this supports our hypothesis, suggesting that exposure to MWCNTs induces cell damage, proved by the reduced membrane integrity and by the smaller number of MCCs displaying spontaneous activity. Moreover, the small group of cells that maintained firing activity presents an increased discharge rate and a smaller AP amplitude, both related to the

lowering of resting potentials. A more positive resting potential reduces the interspike interval required to reach the threshold of AP firing between consecutive spikes and partially inactivates the voltage-gated Na^+ channels that support the AP upstroke, lowering the AP amplitude.

Given that the mechanism of spontaneous firing of MCCs relies on calcium influx through subthreshold L-type Ca^{2+} channels (Marcantoni et al. 2010; Vandael et al. 2010), an increased firing rate might reflect increased cytosolic calcium levels. Increased cytosolic calcium levels are related to cell death and it might be that the faster firing rate after MWCNTs treatment becomes indicative of a pre-apoptotic/necrotic state of the cell. Notice that, Ca^{2+}-dependent pacemaker mechanisms have been associated with the progress of neurodegenerative diseases, such as Parkinson, in dopaminergic neurons of the subtstantia nigra pars compacta (Chan et al. 2007). Paradoxically, a slower K^+ current carried by BK channels, theoretically, should induce more profound hyperpolarizations, leading to decreased firing frequencies. In the literature, however, one can find that the acute block of BK channels by paxilline has opposite effects compared to the chronic block or knock out of BK channels in Purkinje neurons (Sausbier et al. 2004), suggesting that any change to BK channel conductance may lead to different effects on cell firing, depending on the tight coupling with voltage-gated Ca^{2+} channels and levels of intracellular Ca^{2+} regulated by a variety of intracellular pathways. Since our cellular preparations were chronically incubated with MWCNTs, we assume that the potentiating effects on BK channels persisted for prolonged periods. Sustained BK currents could help the cells that maintained their spontaneous firing in AP repolarization and a faster recovery of voltage-gated Ca^{2+} channels that are necessary to restart the AP upstroke. Given the reduced input resistance, it does not necessarily mean that bigger currents lead to more profound membrane voltage changes. We hypothesize that the effects of the MWCNTs-induced membrane damage prevail on the MWCNTs-induced effects on BK currents.

The cytotoxic effect of MWCNTs, highlighted by our work, is in agreement with other papers where they demonstrate that MWCNTs induce a significant dose-dependent decrease of cell viability either in human fibroblasts or NIH 3T3 mouse fibroblasts, block of cell cycle and impaired DNA synthesis (Zhang et al. 2010). Moreover, these authors. reported destruction of actin fibrils and decreased stress fibers after treatment with MWCNTs, pointing out an important damage at the level of the cytoskeleton, in line with our results.

Our findings suggests that health hazard of nanomaterials may develop through different molecular pathways, which not necessarily lead to a reduced functionality of membrane ion channel conductances. Here we demonstrate that carbon nanotubes induce damage at the level of primary chromaffin cell cultures through a dose-dependent process, more evident at higher concentrations (100 and 263 µg/ml). We also observed that MWCNTs can cross the plasma membrane after 24 h incubation, producing disrupting effects at the cytoplasmic level, especially after 48 h. Internalization of MWCNTs leads to an irritation response, which causes the release of pro-inflammatory cytokines as interleukin 8 in human epidermal keratinocytes (Monteiro-Riviere et al. 2005). This could occur also in MCCs but there is no present evidence to support it. An inflammatory response together with the reduced membrane integrity might explain the increased number of non-firing cells after MWCNTs-treatment, but this needs to be tested in future investigations. All these effects need to be carefully considered when planning the diagnostic or therapeutic use of CNTs, highlighting the need of more detailed studies focused on the safer use and production of this material.

Funding information

The work was supported by the Regione Piemonte [grant number D14-2005 to E.C. and CIPE 2006 Project "Nanoparticles: from their impact on the environment and human health to safer production and usage (NANOSAFE)" to B.F.], by the Compagnia San Paolo [grant to the NIS Center] and by the Italian Ministry of Education, University and Research (MIUR), Programmi di Ricerca scientifica di rilevante Interesse Nazionale (PRIN) 2007, prot. 2007FA34TE.

Acknowledgments

We thank Drs. M. Colonna, C. Franchino and A. Renna for discussions and help during the experiments.

References

Al Faraj A, Cieslar K, Lacroix G, Gaillard S, Canet-Soulas E, Crémillieux Y. 2009. In vivo imaging of carbon nanotube biodistribution using magnetic resonance imaging. Nano Lett. 9(3):1023-7.

Belyanskaya L, Weigel S, Hirsch C, Tobler U, Krug HF, Wick P. 2009. Effects of carbon nanotubes on primary neurons and glial cells. Neurotoxicology 30(4):702-11.

Chan CS, Guzman JN, Llijic E, Mercer JN, Rick C, Tkacth T, Meredith GE, Surmeier DJ. 2007. Rejuvenation" protects neurons in mouse models of Parkinson's disease. Nature 447(7148):1081-6.

Deng X, Jia G, Wang H, Sun H, Wang X, Yang S, Wang T, Liu Y. 2007. Translocation and fate of multi-walled carbon nanotubes in vivo. Carbon 45:1419-1424.

Donaldson K, Aitken R, Tran L, Stone V, Duffin R, Forrest G, Alexander A. 2006. Carbon nanotubes: a review of their properties in relation to pulmonary toxicology and workplace safety. Toxicol. Sci. 92(1):5-22.

Donaldson K, Poland CA. 2009. Nanotoxicology: new insights into nanotubes. *Nat.* Nanotechnol. 4(11):708-10.

Dugan LL, Turetsky DM, Du C, Lobner D, Wheeler M, Almli CR, Shen CK, Luh TY, Choi DW, Lin TS. 1997. Carboxyfullerenes as neuroprotective agents. Proc Natl Acad Sci U S A. 94(17):9434-9.

Elder A, Gelein R, Silva V, Feikert T, Opanashuk L, Carter J, Potter R, Maynard A, Ito Y, Finkelstein J, Oberdoster G. 2006. Translocation of inhaled ultrafine manganese oxide particles to the central nervous system. Environ. Health Persp. 114(8):1172-8.

Elgrabli D, Abella-Gallart S, Robidel F, Rogerieux F, Boczkowski J, Lacroix G. 2008. Biodistribution and clearance of instilled carbon nanotubes in rat lung. Toxicol. 253(1-3):131-6.

Elgrabli D, Abella-Gallart S, Aguerre-Chariol O, Robidel F, Rogerieux F, Boczkowski J, Lacroix G. 2007. Effect of BSA on carbon nanotube dispersion for in vivo and in vitro studies. Nanotoxicology. 1(4):266-278.

Fenoglio I, Greco G, Tomatis M, Muller J, Raymundo-Pinero E, Beguin F, Fonseca A, Nagy JB, Lison D, Fubini B. 2008. Structural defects play a major role in the acute lung toxicity of multi-wall carbon nanotubes: physico-chemical aspects. Chem. Res. Toxicol. 21:1690-1697.

Fubini B, Ghiazza M, & Fenoglio I. 2010. Physico-Chemical Features of Engineered Nanoparticles Relevant to Their Toxicity. Nanotoxicology. 4(4): 347–363

Guo L, Morris DG, Liu XY, Vaslet C, Hurt RH, Kane AB. 2007. Iron bioavailability and redox activity in diverse carbon nanotube samples. Chem. Mater. 19(14):3472-3478.

Jakubek LM, Marangoudakis S, Raingo J, Liu X, Lipscombe D, Hurt RH. 2009. The inhibition of neuronal calcium ion channels by trace levels of yttrium released from carbon nanotubes. Biomaterials. 30(31):6351-7.

Jin H, Heller DA, Strano M. 2009. Size-dependent cellular uptake and expulsion of single-walled carbon nanotubes: single particle tracking and a generic uptake molde for manoparticles. ACSNano, 3(1):149-158.

Jorio A, Saito R., Dresselhaus G, Dresselhaus MS. 2004. Determination of nanotubes properties by Raman spectroscopy Philosoph. Trans. Royal Soc. A-Mat. Phys. Engin. Sci., 362: 2311-2336.

Kane AB, Hurt RH. 2008. Nanotoxicology: the asbestos analogy revisited. Nat. Nanotechnol. 3(7):378-9.

Kostarelos K, Lacerda L, Pastorin G, Wy W, Wieckowski S, Luangsivilay J, Godefroy S, Pantarotto D, Briand JP, Muller S et al. 2007. Cellular uptake of functionalized carbon nanotubes is indipendent of funcional group and cell type. Nat. Nanotechnol. Lett.

2(2):108-112.

Kreyling WG, Semmler M, Erbe F, Mayer P, Takenaka S, Schulz H, Oberdörster G, Ziesenis A. 2002. Translocation of ultrafine insoluble iridium particles from lung epithelium to extrapulmonary organs is size dependent but very low. J. Toxicol. Environ. Health A. 65(20):1513-30.

Lam CW, James JT, McCluskey R, Arepalli S, Hunter RL. 2006. A review of carbon nanotube toxicity and assessment of potential occupational and environmental health risks. Crit. Rev. Toxicol. 36(3):189-217.

Lin AMY, Chyi BY, Wang SD, Yu HH, Kanakamma PP, Luh TY, Chou CK and Ho L T. 1999. Carboxyfullerene Prevents Iron-Induced Oxidative Stress in Rat Brain. J. Neurochem 72(4):1634–1640.

Lison D and Muller J. 2008. Lung and systemic responses to carbon nanotubes (CNT) in mice. Toxicol. Sci. 101(1):179-80.

Liu X, Guo L, Morris D, Kane AB, Hurt RH. 2008. Targeted Removal of Bioavailable Metal as a Detoxification Strategy for Carbon Nanotubes. Carbon. 46(3):489-500.

Marcantoni A, Carabelli V, Vandael DH, Comunanza V, Carbone E. 2009. PDE type-4 inhibition increases L-type Ca^{2+} currents, action potential firing, and quantal size of exocytosis in mouse chromaffin cells. Pflügers Archiv Eur J Physiol. 457(5):1093-1110.

Marcantoni A, Vandael DH, Mahapatra S, Carabelli V, Sinnegger-Brauns MJ, Striessnig J, Carbone E. 2010. Loss of Cav1.3 channels reveals the critical role of L-type and BK-channel coupling in pacemaking mouse adrenal chromaffin cells. J. Neurosci. 30(2):491–504.

Monteiro-Riviere NA, Nemanich RJ, Inman AO, Wang YY, Riviere JE. 2005. Multiwalled carbon nanotube interactions with human epidermal keratinocytes. Toxicol. Lett. 155(3):377-384.

Muller J, Huaux F, Fonseca A, Nagy JB, Moreau N, Delos M, Raymundo-Piñero E, Béguin F, Kirsch-Volders M, Fenoglio I, Fubini B, Lison D. 2008. Structural defects play a major role in the acute lung toxicity of multi-wall carbon nanotubes : toxicological aspects. Chem. Res. Toxicol. 21(9):1698-1705.

Muller J, Delos M, Panin N, Rabolli V, Huaux F and Lison D. 2009. Absence of carcinogenic response to multiwall carbon nanotubes in a 2-year bioassay in the peritoneal cavity of the rat. Toxicol. Sci. 110(2):442-448.

Nel A, Xia T, Mädler L, Li N. 2006. Toxic potential of materials at the nanolevel. Science. 311(5761):622-627.

Nemmar A, Vanbilloen H, Hoylaerts MF. 2001. Passage of intratracheally instilled ultrafine particles from the lung into the systemic circulation in hamster. Am. J. Respir. Crit. Care Med. 164(9):1665-8.

Oberdörster, G. 2001. Pulmonary effects of inhaled ultrafine particles. Int. Arch. Occup. Environ. Health. 74(1):1-8.

Oberdörster G, Sharp Z, Atudorei V, Elder A, Gelein R, Lunts A, Kreyling W, Cox C. 2002. Extrapulmonary translocation of ultrafine carbon particles following whole-body inhalation exposure of rats. J. Toxicol. Environ. Health A. 65(20):1531-43.

Oberdörster G, Sharp Z, Atudorei V, Elder A, Gelein R, Kreyling W, Cox C. 2004. Translocation of inhaled ultrafine particles to the brain. Inhal Toxicol. 16(6-7):437-45.

Osswald S., Havel M., Gogotsi, Y. 2007. Monitoring oxidation of multiwalled carbon nanotubes by Raman spectroscopy J. Raman Spectr. 38:728-736.

Park KH, Chhowalla M, Iqbal Z and Sesti F. 2003. Single-walled carbon nanotubes are a new class of ion channel blockers. JBC. 278:50212-50216.

Poland CA, Duffin R, Kinloch I, Maynard A, Wallace WA, Seaton A. 2008. Carbon nanotubes introduced into the abdominal cavity of mice show asbestos-like pathogenicity

in a pilot study. Nat. Nanotechnol. 3(7):423-8.

Raffa V, Ciofani G, Vittorio O, Riggio C, Cuschieri A. 2010. Physicochemical properties affecting cellular uptake of carbon nanotubes. Nanomedicine. 5(1), 89-97.

Ryman-Rasmussen JP, Mark F, Cesta MF, Brody AR, Shipley-Phillips JK, Everitt JI, Tewksbury EW, Moss OR, Wong BA, Dodd DE et al. 2009. Inhaled carbon nanotubes reach the subpleural tissue in mice. Nat. Nanotechnol. 4(11):747-51.

Sausbier M, Hu H, Arntz C, Feil S, Kamm S, Adelsberger H, Sausbier U, Sailer CA, Feil R, Ofmann F et al. 2004. Cerebellar ataxia and purkinje cell dysfunction caused by Ca^{2+}-activated K^{+} channel deficiency. PNAS. 101(25):9474-9478.

Shvedova AA, Kisin ER, Porter D, Schulte P, Kagan VE, Fadeel B, Castranova V. 2009. Mechanisms of pulmonary toxicity and medical applications of carbon nanotubes: Two faces of Janus? Pharmacol. Ther. 121(2):192-204.

Smith PK, Krohn RI, Hermanson GT, Mallia AK, Gartner FH, Provenzano MD, Fujimoto EK, Goeke NM, Olson BJ, Klenk DC. 1985. Measurement of protein using bicinchoninic acid. Anal Biochem 150:76-85.

Sørensen JB, Nagy G, Varoqueaux F, Nehring RB, Brose N, Wilson MC, Neher E. 2003. Differential control of the releasable vesicle pools by SNAP-25 splice variants and SNAP-23. Cell 114(1):75-86.

Takagi A, Hirose A, Nishimura T, Fukumori N, Ogata A, Ohashi N, Kitajima S, Kanno J. 2008. Induction of mesothelioma in p53+/- mouse by intraperitoneal application of multi-wall carbon nanotube. J. Toxicol. Sci. 33(1):105-16.

Xu H, Bai J, Meng J, Hao W, Xu H, Cao JM. 2009. Multiwalled carbon nanotubes suppress potassium channel activities in PC12 cells. Nanotechnology 20(28):285102-285111.

Yu JR, Grossiord N, Koning CE, Loos J. 2007. Characterization of conductive multiwall carbon nanotube/polystyrene composites prepared by latex technology. Carbon

45(15):618-623.

Vandael D, Marcantoni A, Mahapatra S, Caro A, Ruth P, Zuccotti A, Knipper M, Carbone E. 2010. Cav1.3 and BK channel coupling for timing and regulating cell firing. Molecular Neurobiology 42:185-198.

Zhang Y, Wang B, Meng X, Sun G, Gao C. 2010. Influences of Acid-treated Multiwalled carbon nanotubes on fibroblasts: proliferation, adhesion, migration, and wound healing. Ann Biomed Eng. DOI: 10.1007/s10439-010-0151-y.

Figure captions

Fig. 1 – *Transmission Electron Microscopy (TEM) image of ground MWCNTs*. In the inset enlarged view of a single broken nanotube.

Fig. 2 – *Raman spectra of MWCNTs*. Full line pristine MWCNTs, dotted line ground MWCNTs. The positions of the bands are indicated in the upper part of the figure. The band centred at 1340 cm^{-1}, designated as D, is associated to structural defects, while the band at 1570 cm^{-1}, designated as G, corresponds to the tangential in-plane stretching vibration of the carbon-carbon bonds within the graphene sheets. The observed decrease of the relative intensity of the G band indicates the increase of the number of defects during the grinding process.

Fig. 3 – *Dispersion of MWCNTs in culture media.* MWCNTs 263 μg/ml dispersed in DMEM +15% FBS. a) Equivalent hydrodynamic diameter of single CNTs or agglomerates evaluated by dynamic light scattering (DLS). The curves correspond to five measurements made during 15 minutes. b) Optical micrograph of the suspension.

Fig. 4 – *Electron microscopy photographs of cultured RCCs.* a) Image of the cytoplasm of a control chromaffin cell. The black spots highlighted by the white arrow represent the chromaffin granules. b) High magnification of the nuclear (N) and perinuclear region of a chromaffin cell exposed for 24 h to MWCNTs. To the top-left is visible an aggregate outside the nucleus (dashed white lines). The rectangle on the bottom left (white lines) clearly shows a single nanotube crossing the nuclear membrane. c) Image of a chromaffin cell after 48 h of exposure to MWCNTs. The cytoplasm is full of aggregates (one is indicated by the dashed square) and the internal organization of the cell is damaged. d) Image of the cytoplasm of a

chromaffin cell exposed for 48 h to MWCNTs. A couple of single nanotubes is indicated by the black arrows. e) Percentage of internalization of MWCNTs after 24 h (78%) and 48 h (80%) of exposure. f) After 24 h (left panel) the nanotubes inside the cells were either single or in form of aggregates at similar percentages (51% and 49%, respectively). After 48 h (right panel), the percentage of aggregates increased (78%) while decreased that containing single MWCNTs (22%). These percentages were calculated considering the number of cells that internalized MWCNTs as 100% for each group (24 h and 48 h).

Fig. 5 – *MWCNTs reduce the percentage of MCCs with spontaneous activity.* a) Percentage of cells showing spontaneous firing activity in control and treated groups (30, 100 and 263 μg/ml). b) Quantification of membrane input resistance by applying a 100 ms hyperpolarizing current pulse (-10 pA) from resting potential and then measuring the induced voltage change (ΔV), as indicated. Traces were averaged over n= 3 control cells (black) and n= 5 cells treated with 263 μg/ml MWCNTs (grey) obtained from the same culture. c) Membrane input resistance versus MWCNTs concentration. Data are fitted with a dose-response curve with IC_{50}= 37.0 ± 0.5 μg/ml and Hill slope= 3.5 ± 0.2. Differences are statistically significant between control and higher concentrations: 100 and 263 μg/ml (Student's t-test, $p<0.01$ **). d) Linear correlation between the percentage of spontaneously firing MCCs and the input resistance (GΩ), in control and at different MWCNTs concentrations (R= 0.99).

Fig. 6 – *MWCNTs increase the firing frequency of spontaneously active MCCs.* a) Spontaneous action potentials (APs) recorded in current-clamp mode from a control, fullerenes-treated (263 μg/ml) and a 24 h MWCNTs-treated MCCs (263 μg/ml). b) Effects of MWCNTs and fullerenes on the AP amplitude measured as indicated in the top panel. The box diagram shows the mean AP amplitudes at control, with fullerenes and with MWCNTs at

the indicated concentrations. Mean values were: 76.9 ± 1.2 mV, n= 25 (control); 75.6 ± 2.8 mV, n= 8 (fullerenes); 71.8 ± 2.1 mV, n= 7 (MWCNT 30 μg/ml); 70.0 ± 2.2 mV, n= 6 (MWCNT 100 μg/ml); 70.6 ± 3.6 mV, n= 5 (MWCNT 263 μg/ml). c) Linear correlation between baseline values (mV) and firing frequency (Hz) in controls and MWCNTs-treated cells (R= 0.74). d) Firing frequency (Hz) measured at different MWCNTs concentrations (μg/ml) and in controls. At the highest concentration of MWCNTs, data are significantly different from controls ($p< 0.05$).

Fig. 7 – *Voltage-gated Ca^{2+} and Na^{+} currents are not affected by MWCNTs.* a) Na^{+} and Ca^{2+} currents recordings in control and MWCNTs-treated cells following sequential depolarizations of increasing voltages from –50 to +40 mV by 10 mV steps. b) Steady-state Ca^{2+} current amplitudes measured at the end of the pulse, in control MCCs (black squares) and after MWCNTs-treatment (grey circles). c) Quantity of Ca^{2+} charges (pC) at different voltages in control and MWCNTs-treated cells. The amount of Ca^{2+} charge entering the cell was estimated by integrating each current trace for the duration of the pulse, excluding the first 5 ms in which the currents were mainly carried by Na^{+} channels. Data were not statistically different ($p< 0.2$). d) Peak Na^{+} current amplitudes recorded in control conditions and after 24 h MWCNTs treatment. At each voltage, data are not statistically different.

Fig. 8 – *Exposure to MWCNTs promotes a switch from fast-inactivating to noninactivating BK currents.* a) Voltage pulse protocol used to record Kv and BK currents. The first voltage pulse was a step depolarization from –70 mV to +80 mV lasting 400 ms and return to –70 mV. The second pulse was delivered after 10 s and consisted of a pre-step of 20 ms at 0 mV before the test pulse to + 80 mV (filled dot). b) Voltage-clamp recordings in control MCCs. The grey trace represents the voltage-gated Kv current recorded during the first pulse while

the black trace is the BK + Kv current recorded during the second pulse. To the right are the mean amplitudes (nA) of Kv current (grey bar) and BK currents measured at the peak (BKp; black bar) and at the steady-state (BKss; white bar) as indicated in panel c. To the bottom are shown current recordings in the presence of 1 μM paxilline in which is evident the full block of transient BK currents. c) Voltage-clamp recordings in MWCNTs-treated mouse chromaffin cells (24 h). Grey and black traces have the same meaning of those reported in panel b, with the exception that BK currents appear less inactivating. To the bottom are shown current recordings in the presence of 1 μM paxilline in which is evident the full block of transient BK currents. To the right are reported the mean amplitudes of Kv, BKp and BKss as determined in panel b. Only the BKss values were statistically different (*** $p < 0.001$; control vs. MWCNTs using Student's t-test).

Tables

Table 1. Physico-chemical properties of multi-walled carbon nanotubes

samples	Mean diameter (nm)	Mean length (μm)	SSA (m^2/g)	Elemental analysis (% oxides)[c]	Iron potentially bioavailable[d] (% Fe_2O_3)	Amount of defects[e] I_D/I_G
CNT	50÷100 [a]	>10 μm[a]	35.0 ± 0.1	Fe 0.61±0.01 Al 0.04 ±0.05 Co < d.l. Ni 0.003± 0.001	0.43±0.01	0.12±0.03
ground CNT	67±2[b]	1.12±0.05[b]	60.3 ± 0.2	Fe 0.50±0.01 Al 0.06 ±0.03 Co < d.l. Ni < d.l.	0.42±0.01	0.34±0.08

[a] roughly evaluated by SEM
[b] evaluated by TEM
[c] evaluated by means of AE-ICP spectrometry
[d] evaluated by measuring spectrophotometrically the amount of iron ions extracted by ferrozine/ascorbic acid system
[e] evaluated by means of Raman spectroscopy

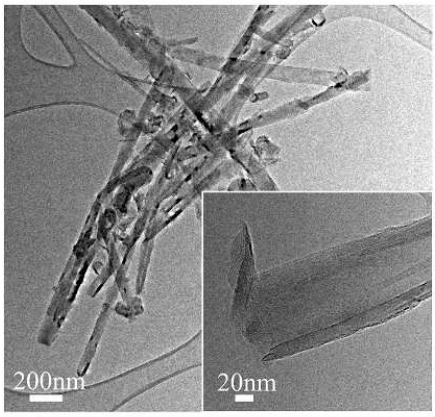

Figure 1

Transmission Electron Microscopy (TEM) image of ground MWCNTs.
254x190mm (96 x 96 DPI)

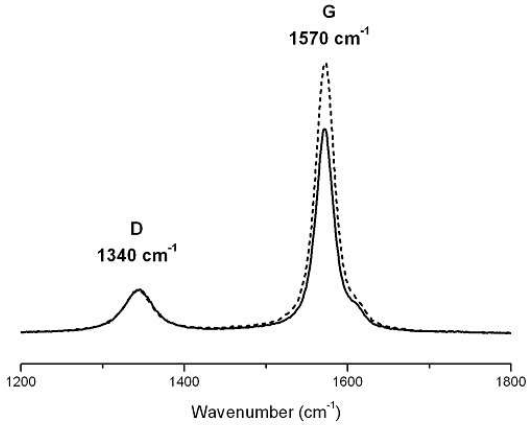

Figure 2

Raman spectra of MWCNTs.
254x190mm (96 x 96 DPI)

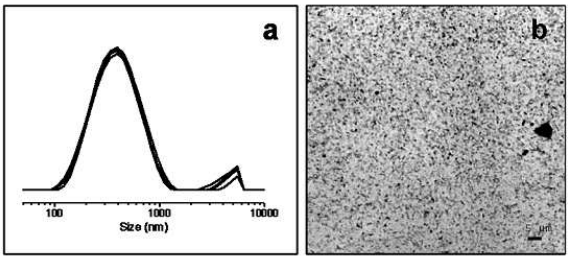

Figure 3

Dispersion of MWCNTs in culture media.
254x190mm (96 x 96 DPI)

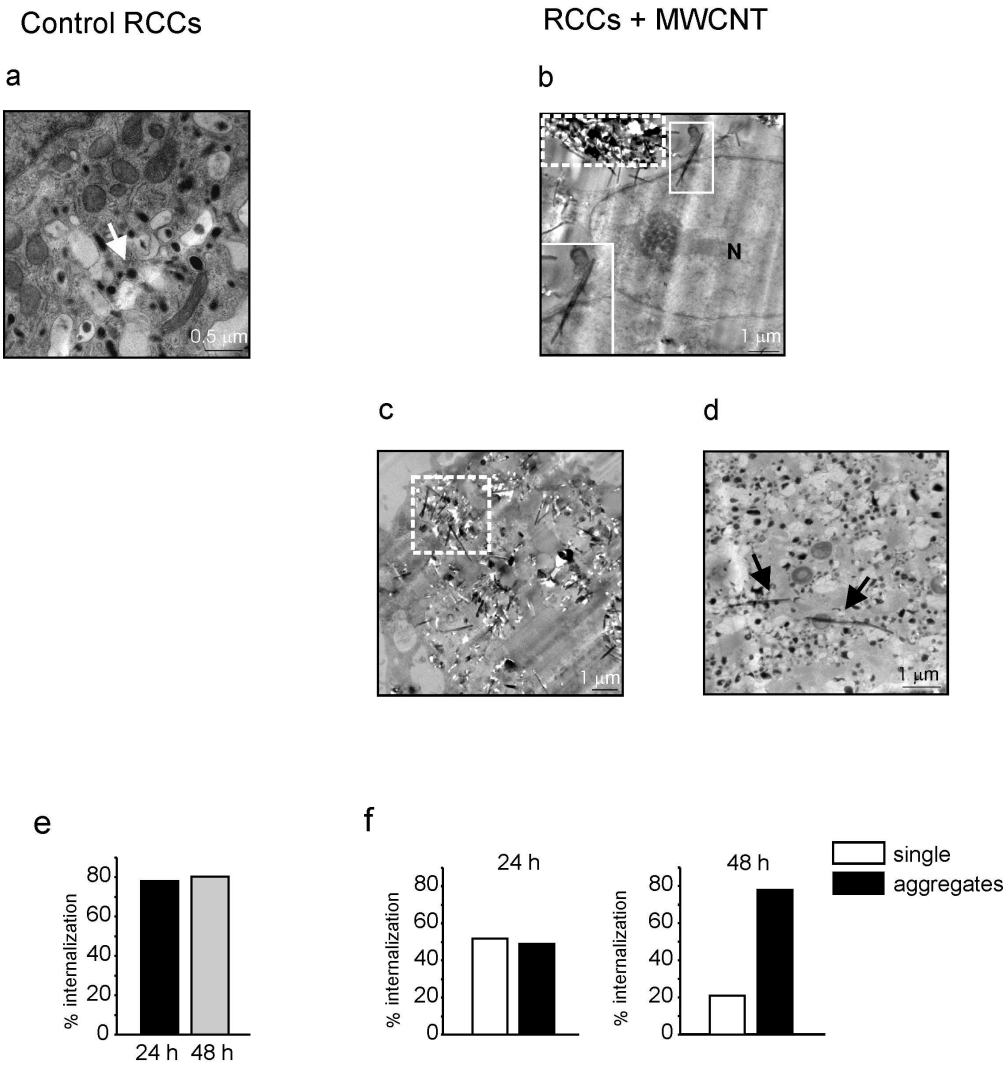

Figure 4

Electron microscopy photographs of cultured RCCs.
191x214mm (300 x 300 DPI)

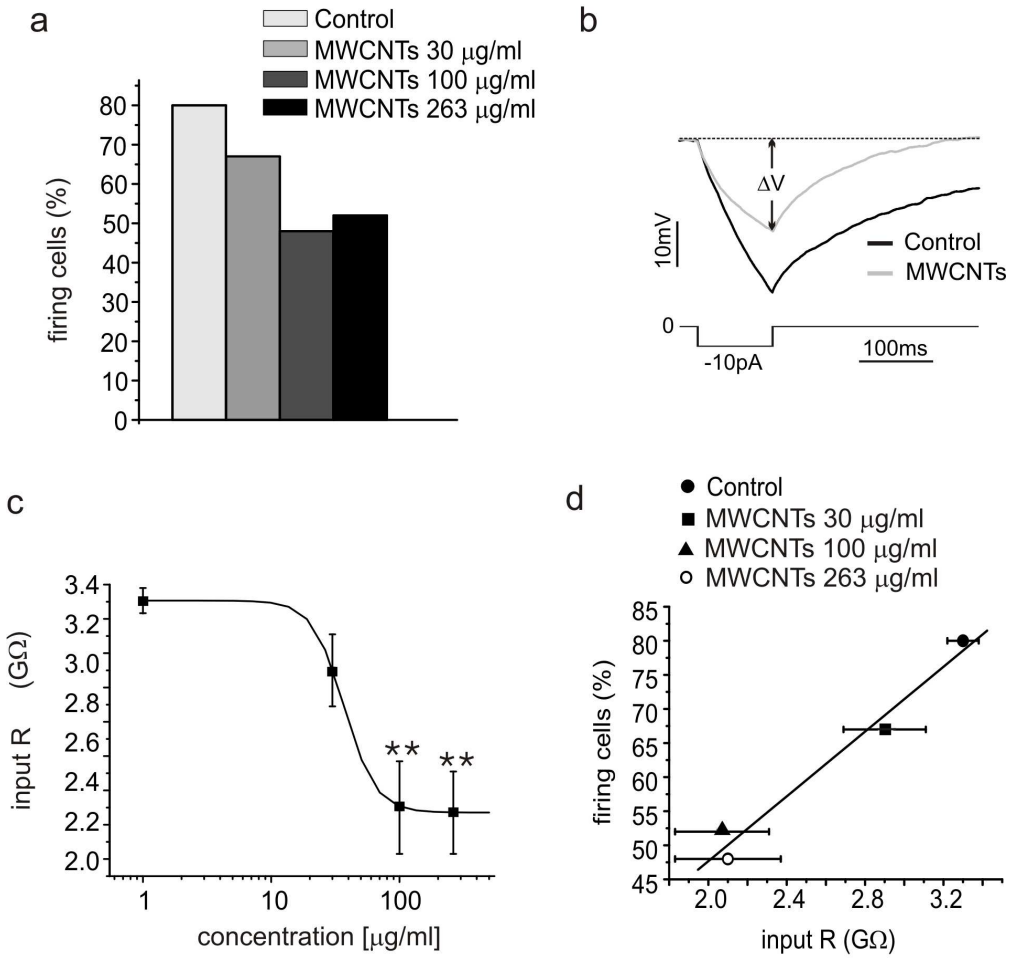

Figure 5

MWCNTs reduce the percentage of MCCs with spontaneous activity.
161x168mm (300 x 300 DPI)

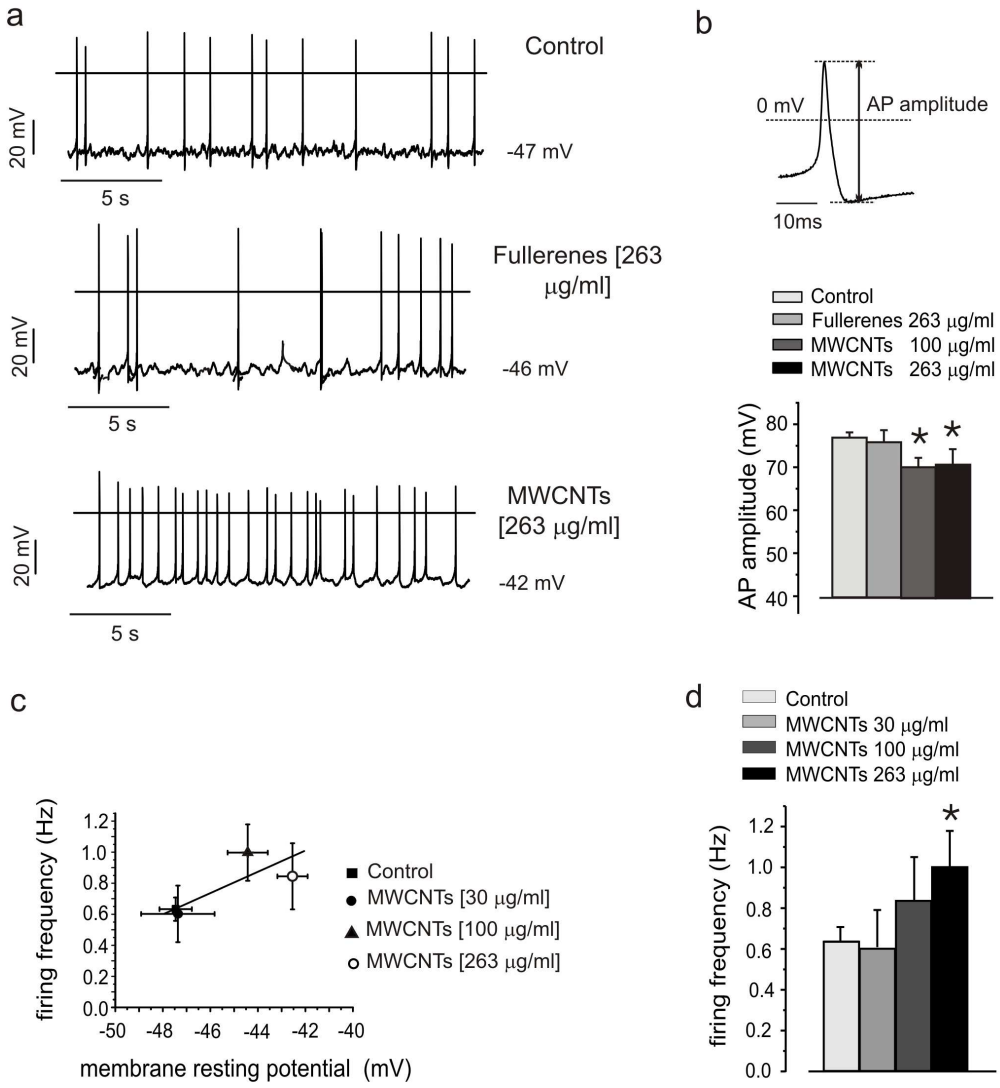

Figure 6

MWCNTs increase the firing frequency of spontaneously active MCCs.
171x199mm (300 x 300 DPI)

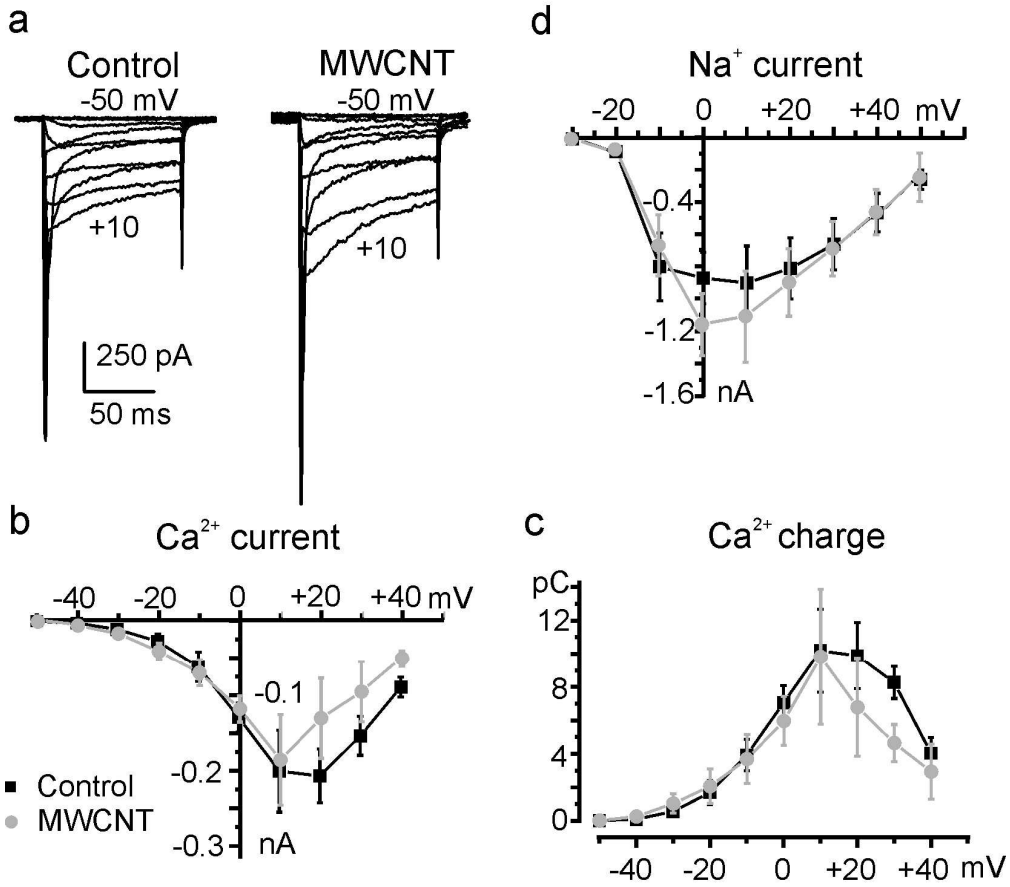

Figure 7

Voltage-gated Ca^{2+} and Na^{+} currents are not affected by MWCNTs.
139x139mm (300 x 300 DPI)

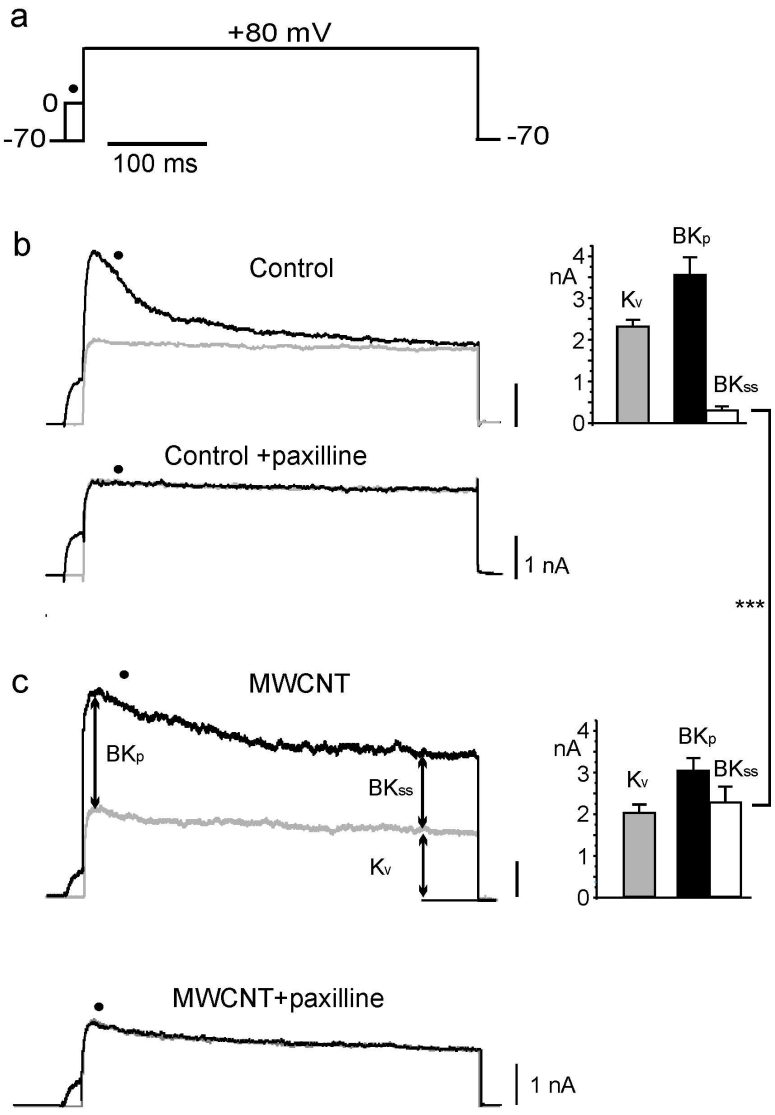

Figure 8

Exposure to MWCNTs promotes a switch from fast-inactivating to noninactivating BK currents.
143x224mm (300 x 300 DPI)